RESEARCH ARTICLE

Synthesis and Characterization of Chitosan/ Soy Protein /Clay Nanocomposite BioFilm for the Release of the Drug

Fatemeh Mirjalili[1*], Mahboobeh Mahmoodi [2,3], Fatemeh Sadeghian-Nodoushan [4,5], Seyyed Ahmad Mirzababaieiy[2]

[1] Department of Material Engineering, Maybod Branch, Islamic Azad University, Maybod, Iran

[2] Department of Biomedical Engineering, Yazd Branch, Islamic Azad University, Yazd, Iran.

[3] Joint Reconstruction Research Center, Tehran University of Medical Sciences, Tehran, Iran

[4] Department of Tissue Engineering research Center, School of advanced technologies in Medicine, Shahid Beheshti University of Medical Science, Tehran, Iran.

[5] Medical Nanotechnology and Tissue Engineering Research Center, Yazd Reproductive Science Institute, Shahid Sadoughi University of Medical Sciences, Yazd, Iran.

ARTICLE INFO

Article History:
Received 2022-05-11
Accepted 2024-06-12
Published 2023-05-05

Keywords:
Chitosan,
Soy protein,
Valsartan,
Nanoclayparticles

ABSTRACT

Soy protein is one of the most easily available biodegradable polymers. However, there are some drawbacks that limit its application. Recently, soy protein-based nanocomposite biofilm has proven to be a promising option for improving properties. In this study, chitosan/ soy protein /clay nanocomposite biofilm containing valsartan as a drug was fabricated by the solvent mixing method. Then, the nanobiofilm properties such as surface morphology, chemical structure, swelling ratio, degradation rate, and release rate of valsartan were measured. The results showed the formation of a chemical bond in the constituents along with a smooth, monolithic, and compact surface. In addition, the swelling and degradation tests indicated that the addition of 0.1 g of clay nanoparticles to the biofilm resulted in an increase in the swelling and biodegradation rate, and with the addition of 0.05 g of nanoclay particles, a significant decrease in the rate of degradation and swelling of the biofilm was observed. The drug release test results also showed that there was no severe release by soy protein /chitosan/clay nanocomposite biofilm containing valsartan, and the drug release indicated a uniform release of nanocomposite biofilms with 0% and 0.05% of nanoclay particles. Then, the MTT assay was evaluated, which showed no cytotoxicity results in any of the nanobiofilms. Therefore, nanocomposite biofilms with 0% and 0.05% of nanoclay may be a more suitable option for valsartan release through the nanocomposite biofilm for lowering the blood pressure.

How to cite this article

Mirjalili F., Mahmoodi M., Sadeghian-Nodoushan F., Mirzababaieiy S.A., Synthesis and Characterization of Chitosan/ Soy Protein /Clay Nanocomposite BioFilm for the Release of the Drug. J. Nanoanalysis., 10 (2): 463-479, Spring 2023.

*Corresponding Author Email: *Fm.mirjalili@gmail.com*

INTRODUCTION

Carrier-mediated drug delivery has emerged as a dominant methodology for the treatment of various pathologies. The therapeutic index of traditional and novel drugs is enhanced via an increase in specificity due to the targeting of drugs to a particular tissue, cell, or intracellular compartment, the control over release kinetics, the protection of the active agent, or a combination of the above [1]. Polymer composites were proposed as drug carriers over 30 years ago and have received growing attention since, mainly due to their stability, enhanced loading capabilities, and control over physicochemical properties [2, 3]. Drug delivery plays an important role in the development of pharmaceutical dosage forms for the healthcare industry because often the duration of the drug release needs to be extended over a period of time [4-7]. This can be completed by the incorporation of drugs into polymeric material to control drug release at a pre-defined and reproducible rate for a prolonged duration. The most important biodegradable polymers that have been used for controlled drug delivery are chitosan, soy protein, gelatin, sodium alginate, PLA, PCL, polyanhydrides, and polyorthoesters [2].

Soybean protein is commercially available in the form of defatted soy four (DSF), soy protein concentrate (SPC), and soy protein isolate (SPI) [8]. Soy proteins consist of both polar and non-polar side chains; therefore, there are strong intra- and inter-molecular interactions. The strong charge and polar interactions between side chains of soy protein molecules restrict segment rotation and molecular mobility, which increase the stiffness, yield point, and tensile strength of soy protein films [9]. Chitosan is derived from the N-deacetylation of chitin and has a few exposed amino groups, which makes it a polyatomic polysaccharide. Due to its gel-forming property, it has been used in the development of various drug delivery systems [10-11].

Chitosan has been extensively investigated for several decades for molecular separation, artificial skin, bone substitutes, and so on, owing to its good mechanical properties, biocompatibility, biodegradability, multiple functional groups, as well as solubility in an aqueous medium. However, its properties, such as thermal stability, hardness, and gas barrier properties, are not good enough to meet those wide ranges of applications. For this reason, the chemical structure of chitosan containing multiple functional groups creates the possibility for new bonding between the chitosan chain and nano-filler particles like clay, silica, and carbon nanotubes [12].

Montmorillonite is an aluminosilicate clay composed of tetrahedral layers of silica stacked between octahedral layers of alumina. Montmorillonite has a large specific surface area and exhibits good adsorption, cation exchange, and drug-carrying capabilities [5, 9]. Recently, bio-nanocomposites have emerged as a new class of material that has proven to be a promising route for improving the mechanical and barrier properties of biopolymers. Bio-nanocomposites consist of a biopolymer matrix reinforced with particles with at least one dimension in the range of 1–100 nm and have improved properties due to the high surface area and high aspect ratio of nanoparticles [13]. Nanocomposites have been studied extensively because many new exciting materials with novel properties were generated as the addition of nanofiller improved the mechanical, physical, thermal, barrier, water resistance, and other properties of soy protein materials. The nanosized fillers can be either organic or inorganic, such as clay (e.g., Montmorillonite (MMT), hectorite, saponite, and laponite), natural biopolymers, natural antimicrobial agents, metals (e.g., silver), and metal oxides (e.g., TiO_2) [14-18]. Nano-sized fillers act as reinforcement, transferring matrix tension and improving mechanical and barrier properties [19-22]. Montmorillonite (MMT) is

extensively used as a nanoparticle for soy protein plastic due to its easy availability at a low cost, abundance in supply, and physical characteristics, including a high elastic modulus (178 GPa), a high surface area (750 m2/g), and a high specific aspect ratio (50-1000) [23-25].

Researchers prepared SPI/Montmorillonite (MMT) bio-nanocomposite films using melt extrusion for the release of the drug ofloxacin. As MMT content increased from 0 to 15%, tensile strength increased due to the high rigidity and aspect ratio of MMT and the interaction of SPI with MMT. However, the percentage of elongation decreased as the MMT content increased from 5% to 15%, as MMT restricted the motion of soy protein molecules in nanocomposite biofilms and the interaction of SPI with MMT [2]. Karen et al. fabricated the soy protein hydrogels with varying weight percentages in water (15, 18, and 20 wt %) without the use of chemical modifiers or crosslinkers. The material properties, drug-releasing capability, and biocompatibility *in vitro* and *in vivo* were assessed [26].

The comfort of fabrication and tailorable properties of soy hydrogels render them a talented biomaterial for tissue engineering and drug delivery applications, principally wound healing. The novelties of this research are the effect of different percentages of nanoclay on preparing the soy protein /chitosan/clay nanocomposite biofilm and the investigation of the morphological and microstructure properties. Moreover, soy protein /chitosan/clay nanocomposite biofilms are characterized in terms of the mixing of the nanocomposite biofilms with different percentages of valsartan. The target of this project is to develop and evaluate the valsartan release in nanocomposite biofilms.

MATERIALS AND METHODS

Materials

Soy protein isolate (Supro 760) with a protein content of 98% (dry basis) was obtained from Protein Technologies International (St. Louis, MO). The nano 666clay (MMT, 100 nm) was obtained from Sahand Clay Products (Iran). Valsartan was gifted by Amin Pharmaceuticals, Schweizerhalle, Switzerland. Chitosan (DDA =73.3%, medium M.W.) and acetic acid (1M) were procured from Sigma-Aldrich.

Synthesis of Soy protein /chitosan/ clay nanocomposite biofilm

An amount of 0.3 g of SPI was dissolved in 18 ml of distilled water with constant magnetic stirring (RW20 digital, IKA, Staufen, Germany) at 50 °C and 200 rpm to prepare the SPI solutions. Next, 0.05 g of valsartan was added to the solution, which was absolutely homogeneous at 50 °C. 0.5 g of chitosan was dissolved in 49.5.0 mL of 1 wt% acetic acid to get a 0.5 wt% solution.

Different percentages of nanoclay were added to the chitosan solution, followed by stirring at 60 °C for 6 h, and added to the SPI solution, completely homogenized without any bubbles, and then poured into Teflon-coated plates. The films were dried at 37 °C for 48 hours. The schematic of the soy protein/ chitosan/ clay nanocomposite biofilm is shown in Fig. 1. The different formulas of the samples are shown in Table 1.

Field emission scanning electron microscopy

Field emission scanning electron microscopy (FE-SEM, VEGA/TESCAN-LMU, Germany) was used to observe the morphologies of collagen-alginate scaffolds. Initially, a thin layer of gold was coated on the samples (5 x 5 mm) that were placed on the adhesive stub. The working voltage of FE-SEM was 10 kV.

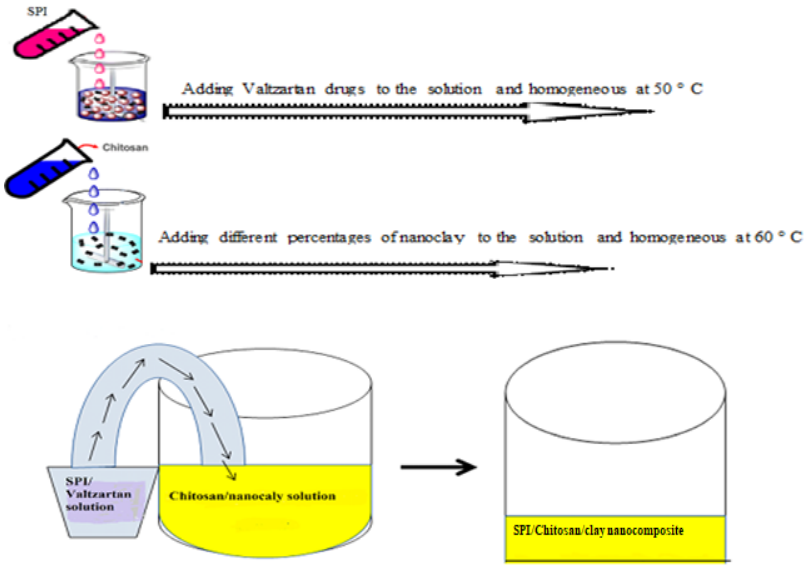

Fig 1. Schematic of Soy Protein/ chitosan/ clay nanocomposite biofilm

Table 1. The formula of Soy Protein /chitosan /clay nanocomposite biofilms

Samples	Chitosan(gr)	Valsartan(gr)	Soy protein (gr)	Nano clay (gr)
H1	0.5	0	0.3	0
H2	0.5	0	0.3	0.1
H3	0.5	0.05	0.3	0.1
H4	0.5	0	0.3	0.05
H5	0.5	0.05	0.3	0.05
H6	0.5	0.05	0.3	0

Fourier-transform infrared spectroscopy

The chemical structures were investigated by using a Fourier transform infrared spectrophotometer (BRUKER-TENOR27, Germany) in the range of 400–4000 cm^{-1}.1 mg of dry sample was mixed with 100 mg of dry KBr, and the mixture was pressed into a disk for spectrum recording.

Swelling studies

The swelling studies of the Soy Protein /chitosan/ clay nanocomposite biofilms were carried out by the following method: The membranes were cut into 1 * 1 cm length and measured for weight (W0). Then, the nanobiocomposites were immersed in 5 ml of simulated body fluid (SBF, pH 7.2) at ambient temperature. After a predetermined time, the samples were removed and the weight (W1) was measured. The swelling rate was calculated using the following equation:

Swelling ratio (R) = (W1-W0/W0) * 100 (1)

In vitro biodegradation

The biodegradation study of the hydrogels was carried out in vitro by incubating the nanocomposite biofilms in pH 7.4 PBS in an incubation dish and keeping them at 37 °C. At a predetermined time interval, the nanocomposite biofilms were taken from the medium, washed with distilled water, and dried. The degradable ratio D was examined by weight loss from the formula:

D = Wo –Wt/ Wo *100% (2)

Where Wo denotes the original weight, while Wt is the

weight at time t: Each biodegradation experiment was repeated three times, and the average value was taken as the percentage of biodegradation.

Determination of drug content

In vitro drug release studies were performed by UV-VIS (V-670PC) spectrophotometry. The amount of valsartan released at different times was calculated using the calibration curve.

For this purpose, four solutions with different concentrations of the valsartan drug were prepared. The first solution contained 2 grams of valsartan drug and was diluted to half of each concentration at each concentration. The calibration curve was plotted according to the concentration of wavelength. The amount of dissolved valsartan drug in the sample taken was measured through a spectrophotometric ally (model-V-670PC, Jasco UV-visible-NIR spectrophotometer) at a λmax of 208 nm [26].

In vitro drug release

The in vitro release of the valsartan drug was carried out using the dialysis bag membrane method. To measure drug release, biofilm samples were prepared in the form of circles with a diameter of 5 cm. The samples were placed in 1 mL of phosphate buffered saline, pH 7.4, maintained at 37 ˚C in the dialysis tube (MW CO 12,000 D, 16 mm diameter, HiMedia, Mumbai, India), and both ends were tightly knotted. The dialysis bag was then placed in 50 mL of PBS at pH 7.4, maintained at 37 ˚C, with constant stirring. The release of the valsartan drug was carried out using 1 mL of PBS maintained at pH 7.4 at 37 ˚C, in which nanobiocomposite film (5 cm^2) was dispersed. Sampling was performed on the first day, once every 10 minutes for the first 30 minutes, followed by three samples with an interval of 30 minutes, two samples with an interval of 1 hour, and two samples with an interval of 2 hours. After that time, sampling was continued every 24 hours until 216 h. At regular time intervals, the supernatant was pipetted out and replaced with equivalent volumes of fresh phosphate buffer solution. The extent of drug release was subsequently evaluated by using a UV-visible spectrophotometer at 208 nm [26-27]. Release percentage can be seen in the following equation:

Release Percentage = abandoned drug concentration / initial drug concentration × 100 (3)

In vitro cytotoxicity

Human foreskin fibroblasts (HFF cells, Royan Institute, Yazd, Iran) were cultured in complete medium (Dulbecco's modified Eagle's medium with 100 U/mL penicillin/streptomycin; Hyclone, USA) under a humid atmosphere of 95% air and 5% CO_2 at 37 °C in an incubator (Memert Jppssplus). The medium was replaced every other day. In this experiment, six different types of biofilms—chitosan and soy protein—were investigated using 24-well plates (gel surface approximately 1 cm) with 10,000 cells after 72 hours. This was performed in accordance with the standards ISO 10993-5, and directly (direct) was performed. Cell proliferation was used to evaluate toxicity with the 3-(4, 5-dimethylthiazol-2-yl)-2, 5-diphenyl tetrazolium bromide (MTT) assay. For this test, 10,000 cells per sample were poured into 50 ml of serum-supplemented media. After three hours, the cells could be cultured on stick samples to be added to the sample surface for covering. This process was similar to that of the control sample.

The cell-culture medium was removed after a specified time (three days), and 100 ml of MTT solution was applied to each well at a concentration of 0.05 mg/ml, and then incubated at 37 °C for 4 h. The supernatants were removed, and 500 µL of a solution of 0.1% HCl and isopropanol was added to dissolve the purple crystals. The dissolved amount of material in isopropanol was identified at 570 nm with an ELISA reader (Convergent EL-Reader 96X, Germany). Wells with more cells showed a higher optical density than

those with fewer cells. Thus, using a specific equation, wells with much higher cell counts can be identified and compared with control samples.

$$Cell\ Viability\% = \frac{ODs}{ODc} \quad (4)$$

ODs: optical density sample; *ODc*: optical density control [28-30].

Statistical analysis

Experiments were performed three times, and the data were expressed as means ± 0.03. Statistical analysis was performed using Anova tests. $p<0.05$ was considered to be indicative of statistical significance.

RESULTS AND DISCUSSION

Determination of microstructure and bonding of samples by FESEM and FTIR

Fig. 2 shows the surface morphology of H1, H2, H3, H4, H5, and H6 nanocomposite biofilms. FESEM images show that the surface of all nanocomposite biofilms was perfectly smooth, which indicated the proper bonding and compatibility between soy protein, chitosan molecules, and other constituents. Fig. 2(a) shows the H1 nanocomposite biofilm image, which identified that the surface of this biofilm was completely homogeneous and smooth. Chitosan has a good ability to bond with other substances due to its different functional groups and large number of hydrogen bonds. There are small cracks on the surface of H1 nanocomposite biofilm that are related to the release of moisture during the drying process. These cracks increased the penetration of liquids into the nanocomposite biofilm, and the rate and speed of inflation increased rapidly, which increased the rate of biofilm degradation.

The surface image of the H2 nanocomposite biofilm is shown in Fig. 2 (b).The surface of this nanocomposite biofilm was also completely smooth and had fewer cracks than the H1 nanocomposite biofilm, which was due to the presence of round and spherical clay particles. The clay particle created small distortions because of the lack of complete solubility in water in the nanocomposite biofilm network during the drying process and created more suitable places than other parts of the nanocomposite biofilm to remove moisture. This factor reduced the formation of cracks in the nanocomposite biofilm surface and increased its degradation rate. The FESEM image of H3 nanocomposite biofilm is shown in Fig. 2 (c). The large and spherical particles of clay could be clearly seen, and this increase was due to the supersaturation of hydrophobic and hydrophilic materials such as clay and valsartan, which in turn increased the grain boundary stress between this particle and nanocomposite biofilm.

The presence of these two materials in the process of making nanocomposite biofilm led to increasing the distortion of the nanocomposite biofilm structure and creating larger cracks in it by reducing the temperature by 60 °C to an ambient temperature. Also, this increase in stress in the nanocomposite biofilm state led to an increase in the bubble trapped inside the nanocomposite biofilm, which in turn caused an increase in the surface crack of this nanocomposite biofilm compared to other nanocomposite biofilms. This increase in cracks increased inflation at a constant rate in this nanocomposite biofilm compared to other nanocomposite biofilms and increased the degradation of this nanocomposite biofilm. As can be seen in H4 nanocomposite biofilm, the decrease in the amount of clay particles compared to H2 nanocomposite biofilm has led to an increase in surface cracks in this nanocomposite biofilm. This increase in cracking could increase its swelling compared to H2 nanocomposite biofilm. Also, reducing the amount of clay particles led to increased compaction and stability of nanocomposite biofilm structures against degradation and leakage of nanocomposite biofilm bonds, which led to increased nanocomposite biofilm resistance to degradation. However, the number of

surface cracks in H4 nanocomposite biofilm was much less than that in H3 nanocomposite biofilm, which led to a decrease in inflation and an increase in resistance to degradation compared to H3 nanocomposite biofilm.

The surface image of the H5 nanocomposite biofilm is shown in Fig. 2(e). The reduction of clay particles in this nanocomposite biofilm compared to H3 nanocomposite biofilm has led to a significant reduction in the number of surface cracks. Also, the reduction of clay particles has led to an increase in the state of valsartan and a reduction in grain boundary stresses, which created a much more stable structure with a lower surface crack than other nanocomposite biofilms. As a result, the rate of inflation and degradation in this biofilm was drastically reduced, resulting in a slower release. Fig. 2 (f) shows the image of the H6 nanocomposite biofilm with a more uniform surface because of the lack of clay particles, such as in the H1 nanocomposite biofilm. The absence of clay particles managed to increase the solubility of valsartan. This increase in solubility led to increased resistance to moisture and air trapped in the biofilm and raised surface cracks, even in part of the nanocomposite biofilm, to surface layering. These conditions increased the rate of inflation and nanocomposite biofilm degradation.

Fig. 2(g) shows the FTIR spectra of H1, H2, H3, H4, H5, and H6 nanocomposite biofilms in the wavelength range of 400-4000 cm^{-1}. The vibrational peak appearing at a wavelength of 3449 cm^{-1} represented the hydroxyl (OH) and amine (NH) groups in chitosan [26-29]. The peak in wave number 2925 cm^{-1} signified the NH_3^+ group, and the absorption band in wave number 2858 cm^{-1} denoted the CH group. The observed vibrations of wave numbers of 1649, 1149, and 1119 cm^{-1} were related to (C-N), (C-C), and (CH_3) groups in chitosan, respectively [30-31]. The observed vibrations in the wavenumbers of 1600 to 1700 cm^{-1} indicated the amide I group. The peaks in the range of 1150 to 1550 cm^{-1} wavelength were related to the NH amide II bond presented in the soy protein. Also, peaks observed in the range of 1300 to 1450 cm^{-1} were related to C-N and N-H amide III bonds in soy protein [32-34]. The observed vibrations at wavelengths of 862 and 1038 cm^{-1} are related to the Al-Mg-OH and Si-O functional groups in clay particles, respectively [35-38]. The presence and slight fluctuation of the above bonds indicated the presence and establishment of bonds between the constituents of hydrogels.

Swelling and biodegradability properties of samples

Previous studies have shown that increasing the amount of hydrophilic polymer increases the adhesion of nanocomposite biofilm to the mucous membrane [36]. Swelling could control the rate at which the drug was released. In this way, with the increase in inflation, the rate of destruction increased, and as a result of the destruction of the nanocomposite biofilm, drugs were delivered. If the penetration of the solution and the swelling were low, the rate of destruction would be reduced, and consequently, the amount of drug released would be drastically reduced. Excessive swelling also increased the rate of degradation owing to the pressure created by excessive adsorption of the solution. This growth in degradation increased the initial explosive release and raised the release rate. At the same time, excessive swelling of the nanocomposite biofilm could reduce the patient's satisfaction with the use of nanocomposite biofilm or increase the risk of nanocomposite biofilm separating from the mucosal surface and entering the stomach. An excessive increase in swelling also greatly increased the risk of the drug leaving the treatment valve. Thus, in the first hours of placing the nanocomposite biofilm on the mucosa, the released drug might be higher than the toxic dose, or in the last hours, the amount of drug released from the nanocomposite biofilm might be lower than the effective dose. Therefore, balanced inflation increased the efficiency of drug delivery [25-26, 37].

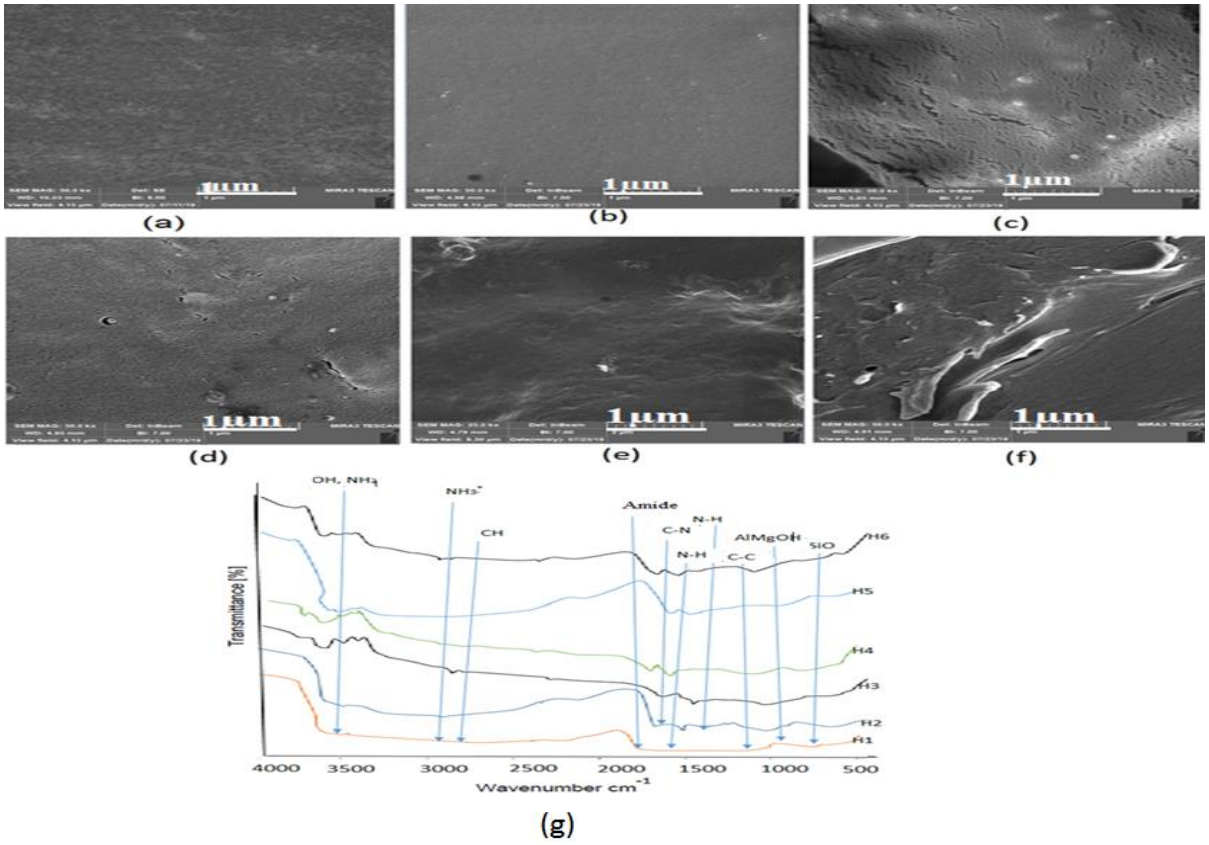

Fig. 2. FESEM images: a) image H1, b) image H2, c) image H3, d) image H4, e) image, f) image H6, and g) FTIR spectrum of H1, H2, H3, H4, H5, and H6 nanocomposite biofilms

Fig. 3(a) shows the swelling curve of H1-H6 nanocomposite biofilms. As can be seen in Fig. 3, the diagram was divided into four parts based on the slope. The first slope of the chart increased sharply due to the rapid penetration of the solution into the nanobiofilm through the surface cracks and the rapid absorption of the solution by the nanocomposite biofilm, and the swelling rate was about 600 percent. Next, the slope of the chart decreased severely, and after 15 minutes, the swelling rate was 650%. This decrease in slope was owing to the resistance of the compact structures of the nanocomposite biofilm against the penetration of the solution. In the next 5 minutes, the slope of the graph increased due to the destruction of compact structures and the rapid penetration of the solution into them. After this period, the slope of the graph became negative because of the increased destruction and the beginning of the outflow of broken bonds. The results at this stage indicated that the rate of severe swelling did not decrease, even after 40 minutes from the start, and the inflation rate was about 600%. This lack of inflation, despite the continued destruction and increase in weight loss, was attributed to the increase in the rate of removal of isolated parts of the nanocomposite biofilm, which indicated a growth in the inflationary strength of the nanobiofilm.

According to the slope of the chart of H2 nanocomposite biofilm and the rate of swelling, the chart could also be divided into four parts. Up to 5 minutes, the slope of the graph increased sharply, and the swelling rate in this area was 180%. Comparison of this part with the first part of the H1 nanocomposite biofilm showed that the reduction of surface cracks in H2 nanocomposite biofilm compared to H1 nanocomposite biofilm led to a significant reduction in inflation in this part of the H2 nanocomposite biofilm.

Subsequently, the slope of the chart has decreased significantly as a result of the weakening of the bonds and breaking them due to the presence of clay particles. Clay particles caused distortion in the compact structures of the nanobiofilm and led to an increase in the rate of disintegration of the bonds during filling and swelling of the compacted parts. As it can be seen, the slope of the graph from 15 to 20 minutes increased because of the resistance of the more compact internal structures to degradation and continued swelling of the nanocomposite biofilm, and then the graph became negative, which showed the destruction of the internal parts to a significant reduction in the amount of film turbulence. After 30 minutes, the swelling rate had decreased to 100%.

A comparison of H2 and H1 nanocomposite biofilms showed that the presence of clay particles caused distortion in the compact structure of the nanocomposite biofilm due to the bond between the two hydrophilic and hydrophobic materials, which significantly reduced the swelling power of H2 nanocomposite biofilm. The obtained results were completely consistent with the results of the FESEM test, which showed that the surface of H2 nanocomposite biofilm had less surface cracking than nanocomposite biofilm and confirmed the presence of globular clay particles inside H2 nanobiofilm. The swelling rate of H3 nanobiofilm in Fig. 4 shows that the percentage of swelling in the first 10 minutes has increased rapidly owing to the presence of many surface cracks in this nanobiofilm, so that, after this period, the swelling rate of the nanobiofilm was 600%. This significant increase in swelling slope compared to other nanocomposite biofilms tested was because of the presence of valsartan particles inside the nanocomposite biofilm, which led to an increase in the compaction of the nanocomposite biofilm structures.

At this stage, the solution dissolved the surface bonds of the nanocomposite biofilm and expanded them resulting, in the surface bonds being completely saturated with the solution. In the next 5 minutes, the slope of the inflation chart decreased quite dramatically. After a time interval of 15 to 25 minutes, due to the structural distortions of clay nanoparticles, the compact internal structures were damaged, and the solution quickly penetrated into them and increased the swelling. To facilitate, in the next 10 minutes, the swelling rate was 1600% of the initial weight before the test. After 25 minutes, the slope of the inflation chart dramatically became negative, attributable to the increase in weaker bond breakage and the outflow of the internal parts of the biofilm. The slope of the chart was almost fixed after 80 minutes. This stabilization of the swelling slope, along with the continued destruction of the bonds and the outflow of the most bonds, showed an increase in the swelling rate of the nanocomposite biofilm. A comparison of the H3 nanocomposite biofilm swelling chart with other samples showed an increase in the swelling of this nanocomposite biofilm compared to other samples under study. This increase in swelling was in complete agreement with the results of the FESEM images, which indicated the presence of more surface cracks in this sample than in other samples.

The swelling chart of H4 nanocomposite biofilm showed that, in the first 5 minutes, the slope of the intensity chart increased, and the swelling rate was 455%. After this period, the slope of the chart decreased significantly, and the rate of swelling was 600 percent after 35 minutes. Then, the diagram showed a significant increase because of the destruction of compact internal structures and the penetration of the solution into them, so that, after 45 minutes, the swelling rate was 1117%. After this period, the slope of the swelling chart became negative, and the slope of the chart was almost fixed after 80 minutes, indicating that inflation and destruction continued. A comparison of the inflation charts of H4 and H2 nanocomposite biofilms showed an increase in the stability of internal compact structures and a

reduction in distortion in compact structures as a result of the reduction of clay particles in H4 nanocomposite biofilms compared to H2 nanocomposite biofilm. Also, this decrease in clay particles has led to an increase in surface cracks and an increase in swelling rate in the first minutes of H4 nanocomposite biofilm compared to H2 nanocomposite biofilm. The results were in complete agreement with the FESEM results, which indicated that there were more surface cracks in the H4 nanocomposite biofilm than in the H2 nanocomposite biofilm.

The H5 nanocomposite biofilm swelling diagram in Fig. 3 shows the slope of the diagram in different parts directed to the formation of several separable parts. In the first part, after 5 minutes, the slope of the chart has increased significantly, and during this period, the inflation rate has reached 300%. This was due to the increase in adsorption, and the rapid absorption of the solution by the nanobiofilm was due to the penetration of the solution through surface cracks. From 5 to 20 minutes, the slope of the graph has decreased to 350%, which is the reason for the resistance of compact structures against the penetration of the solution into them. This nanobiofilm had a higher structural compaction than H2, H3, and H4 nanocomposite biofilms due to the presence of valsartan particles and the reduction of clay particles.

This agent prevented the solution from penetrating into the nanobiofilm after 20 minutes. In the next stage, after 20 to 35 minutes, the slope of the chart has increased to 650% because of the collapse of the compact surface structures of the nanocomposite biofilm and the penetration of the solution into them, along with the stability of the destroyed structures against the exit of the nanocomposite biofilm.

After 35 minutes, the slope of the chart became negative, attributable to the breaking of internal bonds and the exit of parts from the biofilm to the outside, along with the continued resistance of the more compact internal parts to intrusion. Comparison of H5 nanocomposite biofilm with other nanocomposite biofilms indicated an increase in the solubility of valsartan because of the reduction of clay particles, which meaningfully increased the strength of compact structures and reduced the structure compared to other nanobiofilms. From the beginning of the test to 5 minutes, the swelling slop of the H6 nanocomposite biofilm was very high, about 480%, and from 5 to 25 minutes, the slope of the graph decreased to 600%. This phenomenon was due to the resistance of compact structures to the penetration of solution into them and the resistance of broken bonds to leaving the nanocomposite biofilm. The slope of the chart after 25 minutes has decreased, and after 45 minutes, the swelling rate is 520%. The results obtained from this test were in complete agreement with the results of the FESEM test, which indicated that there was a more compact surface at the level of this biofilm. Swelling analysis of the soy protein /chitosan/clay nanocomposite biofilms demonstrated $p > 0.05$, indicating that the quadratic model was not significant in the swelling and biodegradation of each nanocomposite biofilm. Fig. 3(b) shows the degradation diagram of nanobiofilms.

According to the slope of the curve of H1 nanocomposite biofilm, the diagram was divided into several separable parts. Up to 5 minutes after the start of the test, the slope of the graph showed a significant increase, which was due to the destruction of weak bonds on the surface of this nanocomposite biofilm because of the penetration of the solution from surface cracks and the onset of swelling. After that, the slope of the degradation diagram almost proved the resistance of other surface bonds of this nanocomposite biofilm against the continued penetration of the solution into the nanocomposite biofilm, which prevented the solution from reaching the internal structures, and as a result, the degradation rate was significantly reduced. However, by continuing the pressure of the solution and increasing it to penetrate

into the nanobiofilm, these bonds were broken, and the solution penetrated into the nanobiofilm after 15 minutes. After breaking the surface bonds, the amount of swelling and destruction showed a relative increase.

This relative increase in degradation was a result of the resistance of the compact internal structures to the penetration of the solution into them, along with the exit of the broken bonds from the nanocomposite biofilm. So, from 15 to 75 minutes, the rate of destruction has increased from 5% to 13%. After 75 minutes, the slope of the chart showed a substantial increase. During this period, the compact internal structures have collapsed, and the outflow of broken bonds has increased. However, after 180 minutes, the maximum amount of degradation was 25%, which showed the resistance of internal compact structures to degradation after this period. The obtained results were in complete agreement with the results of inflation and FESEM tests, which indicated the presence of surface cracks and a compact structure that prevented high inflation of the biofilm.

The slope of the H2 nanocomposite biofilm degradation chart was incremental after 5 minutes, and 11% of the nanocomposite biofilm has been destroyed because of the presence of surface cracks on account of clay particles. Then, the slope of the condensed graph of nanocomposite biofilm destruction continued with a gentler slope, and after 20 minutes, the rate of nanocomposite biofilm destruction was 22%. This phenomenon was owing to the gradual withdrawal of previously destroyed structures from intrusion and destruction. After 20 minutes, the slope of the chart increased significantly, and after 30 minutes, 80% of the nanocomposite biofilm had been destroyed. This phenomenon was due to the complete destruction of film structures. The results of the degradation test were fully consistent with the results of inflation, which indicated a significant increase in inflation over a period of 15 to 20 minutes.

Examination of the slope of the H3 nanocomposite biofilm degradation diagram showed an increasing slope of the diagram in the first 5 minutes of the test. Therefore, the rate of nanocomposite biofilm destruction was about 6%, attributable to the presence of surface cracks and rapid penetration of the solution into the film, which broke the weak bonds of the nanocomposite biofilm during this period. After this period, up to 15 minutes, the slope of the diagram was reduced because of the resistance of compact structures to the penetration and exit of broken joints, and the destruction rate reached 8% of the nanocomposite biofilm after 15 minutes. In a period of 15 to 20 minutes, the slope of the graph increased, and after 20 minutes, the slope of the graph decreased owing to the resistance of the compact structures to the exit of the broken joints. But since then, the slope of the graph has increased, in addition to the rate of destruction of 41% of the nanobiofilm after 90 minutes.

A comparison of the degradation diagrams of H3 and H2 nanocomposite biofilms showed an increase in resistance to degradation attributable to the presence of valsartan particles inside the H3 nanocomposite biofilm. Also, the comparison of nanobiofilms of H1 and H3 nanocomposite biofilms identified a decrease in resistance to degradation on account of the presence of hydrophobic clay particles in the structure of the H3 nanocomposite biofilm network. The results obtained with the results of inflation tests and FESEM images indicated the presence of surface cracks in H3 nanocomposite biofilm compared to other nanocomposite biofilms, along with the highest rate of swelling in the period of 20 to 30 minutes.

The degradation diagram of H4 nanocomposite biofilm is shown in Fig. 3(b). Examination of the degradation diagram of this nanocomposite biofilm showed an increasing slope of the approximation diagram in the 10 minutes of the test, and 13% of the nanocomposite biofilm has been

destroyed. This amount of degradation was due to the increase in surface cracks, the decrease in the amount of clay particles, and the absence of valsartan particles compared to H3 nanocomposite biofilm. Also, the presence of clay particles in the structure caused distortion in the nanocomposite biofilm structure and increased the initial degradation of H4 compared to H1 nanocomposite biofilm. After 10 minutes, the slope of the chart decreased, and after 75 minutes, the destruction rate had reached 23%.

This occurrence was due to the resistance of internal structures against the penetration of the solution into the nanocomposite biofilm, in addition to preventing the broken bonds from leaving the nanobiofilm. But after 75 minutes, the slope of the chart increased, and 31% of the nanocomposite biofilm was destroyed after 90 minutes. Subsequently, the rate of nanocomposite biofilm destruction was about 40%. After 180 minutes, comparison of degradation diagrams of H3 and H4 nanocomposite biofilms showed an increase in resistance to H4 nanocomposite biofilm degradation by reason of a decrease in the amount of clay particles. The obtained results were in complete agreement with the results of the inflation test, which indicated an increase in the inflation of H3 nanocomposite biofilm compared to H4 nanocomposite biofilm. Investigation of H5 nanocomposite biofilm degradation indicated an increasing slope of the graph in the first 5 minutes with a destruction rate of 3.5% of nanocomposite biofilm. This reduction in initial degradation compared to other films was attributable to the reduction in the amount of clay particles along with the presence of valsartan particles, which increased the strength of compact structures to reduce distortion caused by the presence of clay particles.

The slope of the graph was reduced from 5 to 75 minutes. After this period, the rate of destruction has reached 10% by reason of the resistance of compact structures in contradiction to the penetration of the solution and the failure of bonds. After 75 minutes, the slope of the graph increased by reason of the partial destruction of compact structures and the increased outflow of broken joints. Therefore, after 180 minutes, 24% of the nanocomposite biofilm has been destroyed. The nanocomposite biofilm degradation diagram showed the least amount of degradation in H5 nanocomposite biofilm compared to other nanocomposite biofilms. This amount of analysis could cause a drug release system with a very low explosive release rate and more controlled release than other nanocomposite biofilms studied. The results of the H5 nanocomposite biofilm degradation test were consistent with the results of the swelling test and FESEM images, which showed fewer surface cracks and the least amount of swelling in the H5 nanocomposite biofilm.

The degradation diagram of the H6 nanocomposite biofilm showed the steep slope of the diagram in the first 10 minutes, and during this period, the slope of the chart was 7.2%. Comparison of the degradation diagrams of H5 and H6 nanocomposite biofilms showed that the rate of nanocomposite biofilm degradation of H6 nanocomposite biofilms was higher than that of other nanocomposite biofilms, which was due to the presence of more surface cracks in this nanocomposite biofilm than in the H5 nanocomposite biofilm. After that, the slope of the chart decreased over a period of 10 to 120 minutes, and the rate of destruction was about 16% after 120 minutes, which was on account of the absence of clay particles along with the presence of valsartan particles in the nanobiofilm. After 180 minutes, the rate of destruction of this nanocomposite biofilm reached 40%. This sudden increase was due to the destruction of compact structures and their exit from the nanobiofilm. In the comparison of H5 and H6 nanocomposite biofilms, the degradation graphs showed faster degradation of the H6 nanocomposite biofilm in 120 to 180 minutes. This increase in the strength of H5 nanocomposite biofilm

compared to H6 nanocomposite biofilm was due to the presence of large particles inside the H5 nanocomposite biofilm, which prevented large pieces of nanocomposite biofilm from escaping.

However, the increase in clay particles in the H2 nanocomposite biofilm and the H3 nanocomposite biofilm has increased the amount of trapped air and created structural distortion. These factors weaken the compact structures of these nanobiofilms. Therefore, they had a significant difference from the start of the test.

Investigation of drug release from samples

Valsartan calibration can be seen in the following equation:

$$y = mx + b \quad (5)$$

In the above equation, y represented the drug concentration, x represented the fine surface of the curve, m represented the slope of the line, and b represented the width characteristic of the origin [27, 39].

Fig. 4(a) displays the calibration curve of Valsartan obtained from UV spectrophotometric analysis using a UV spectrophotometer at a wavelength of 208 nm. The absorbance values were recorded.

The percentage release of valsartan from H3, H5, and H6 nanocomposite biofilms is shown in Fig. 4(b) over 2 h. The results showed an explosive release of 4% of H3 nanocomposite biofilm in the first 45 minutes. Also, the rate of explosive release during this period for H5 and H6 nanocomposite biofilms was equal to 1.9 and 1.7. The results indicated a higher explosive release of H3 nanocomposite biofilm than the other two nanobiofilms. After this period, the slope of all three graphs was reduced and fixed. However, the results did not support significant explosive release in any of the nanocomposite biofilms.

Fig. 4(b) shows the release rate of valsartan in three nanocomposite biofilms over a period of seven days. Examination of this chart showed a 10% explosive release from the H3 nanocomposite biofilm in the first 24 hours of the test. The outcomes also presented a volatile release of 7.5% and 7.3% of H5 and H6 nanocomposite biofilms within 24 hours after

Examination of the results did not show any significant differences between these three nanocomposite biofilms in the first 24 hours of the test.

The release rate of H3 nanocomposite biofilm compared to the other two nanocomposite biofilms displayed a significant increase attributable to the increase in the amount of clay particles in this nanocomposite biofilm, which caused a lot of distortion in the structure of this nanobiofilm. The results of the H5 and H6 nanocomposite biofilm release tests did not show any significant differences. The outcomes were wholly consistent with the results of swelling and degradation tests and indicated an increase in the rate of inflation and degradation of H3 nanocomposite biofilm compared to the other two nanocomposite biofilms.

In vitro cytotoxicity

Fig. 5 shows the results of the MTT test, which did not display any cytotoxicity. The results presented 88% and 200% cell growth in soy protein and chitosan samples, respectively. Nanocomposite biofilm samples of H1, H2, H3, H4, H5, and H6 had 97%, 105%, 116%, 120%, 125%, and 128% survival rates, respectively, which was higher than the control sample. Cell viability in H5 and H6 nanocomposite biofilms was higher than that in H3 nanocomposite biofilm, which was related to increased adhesion owing to the control and gradual release of valsartan from H5 and H6 nanocomposite biofilms. However, this difference could be ignored.

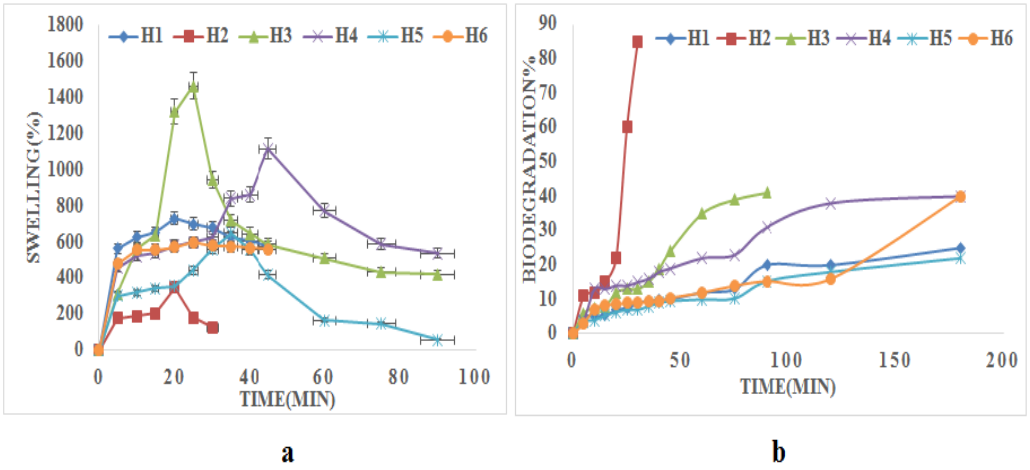

Fig. 3. The swelling (a) and biodegradability (b) properties of H1, H2, H3, H4, H5, and H6 nanocomposite biofilms with a P value < 0.05

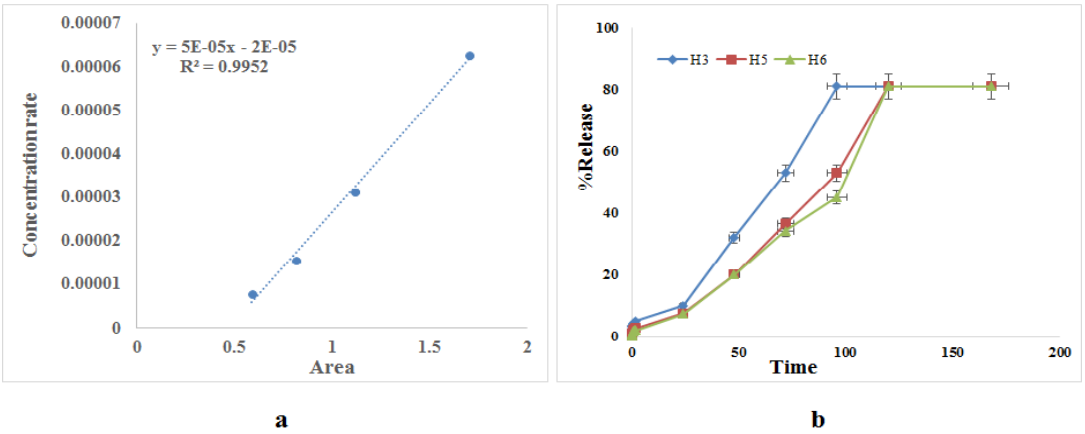

Fig. 4. Calibration curve of valsartan (a) and percentage release of valsartan from nanocomposite biofilms of H3, H5 and H6 (b)

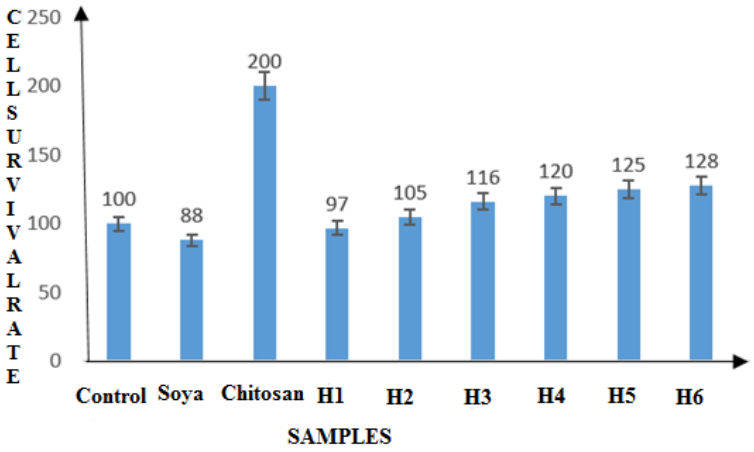

Fig 5. MTT cell survival test for all samples (p<.05 vs. control)

CONCLUSION

In this study, chitosan / soy protein / clay nanocomposite biofilms with targeted delivery and release of valsartan were prepared. Chitosan was used as the background phase due to the excellent absorption of secretions and the formation of a suitable adhesive mucosa in the nanocomposite biofilm. Soy protein was also used as a booster phase that controls the release rate from the nanocomposite biofilm.

Examination of FESEM images showed a good bond between the ingredients and the surface moisture. The number of cracks was inversely related to the proportion of clay particles. The outcomes of the infrared spectroscopy test presented a chemical bond between the constituents of nanocomposite biofilms. Comparing the swelling charts of nanocomposite biofilms showed the lowest inflation rate and the most stable structure for H5 and H6 nanocomposite biofilms. H3 nanocomposite biofilms exhibited the highest swelling rate. Comparison of nanocomposite biofilm degradation results indicated the highest degradation in H2 nanocomposite biofilm and the lowest in H5 nanocomposite biofilm.

Drug release test results showed no high explosive release in any nanocomposite biofilms. The results of the drug release test showed controlled and gradual release in H5 and H6 nanocomposite biofilms compared to H3 nanocomposite biofilm. Cell viability in H5 and H6 nanocomposite biofilms was higher than that in H3 nanocomposite biofilms, which was related to increased adhesion owing to the control and gradual release of valsartan from H5 and H6 nanocomposite biofilms.

REFERENCES

[1] Tarkhan M, Safarina M , Khosh. Effectiveness of Group Stress Inoculation Training on the Systolic and Diastolic Blood Pressure and Life Quality of Hypertension in Women. Quartely Journal of heal psychology. 2012 ; 1;46 - 58.

[2] Preetishree N, Sanjib Kumar S, Anamika B. Synthesis and Characterization of Soy Protein Isolate/MMT Nanocomposite Film for the Control Release of the Drug Ofloxacin. World Journal of Nano Science and Engineering.2011; 1:27-36

[3] Michel I.Guidelines of the French Society of Otorhinolaryngology (SFORL). Epistaxis and high blood pressure. European annals of otorhinolaryngology, Head and Neck Diseases.2017; 134.1: 33-35.

[4] Safaeian L, Zabolian H. Antihypertensive Effect of Lactoferrin on Dexamethasone-Induced Hypertension in Rat. Journal of Isfahan Medical School. 2013; 31(245):1096-1104.

[5] Zarneshan A. Synergic Effect of Aerobic Exercise Training (moderate intensity) and Soy Intake on Blood Pressure and Rest Heart Rate in Obese Postmenopausal Women. Hormozgan Medical Journal.2014; 18.1: 52-60.

[6] Khedr M, Waly A.I, Hafez A.A.H. Synthesis of Modified Chitosan-Montmorillonite Nanocomposite. Aus. J. Basic App. Sci. 2012; 6:216-226.

[7] Wen-Fu L, Yung-Chu C. Effect of Intercalated Hydrotalcite on Swelling and Mechanical Behavior for Poly(acryl acid-co-N-isopropylacrylamide)/Hydrotalcite Nanocomposite Hydrogels . Applied polymer. 2005; 98:1572-1580.

[8] Su J F , Huang Z,Yuan X Y , Wang X Y , Li M. Structure and Properties of Carboxymethyl Cellulose/Soy Protein Isolate Blend Edible Films Crosslinked by Maillard Reactions. Carbohydrate polymers. 2010 ; 79(1): 145-153.

[9] Garima T, Amrinder S, Inderbir S. Chitosan-Montmorillonite Polymer Composites: Formulation and Evaluation of Sustained Release Tablets of Aceclofenac. Sci. Pharm. 2016; 84: 603–617.

[10] Chhavi M, Deepmala KM, Singh VK, Sakshi C, Naman J. Soy Protein Based Green Composite: A

Review. Research & Reviews: Journal of Material Sciences. 2017;1-13.

[11] Khedr M A, Waly A, Hafez A A H. Synthesis of modified chitosan-montmorillonite nanocomposite. Aus. J. Basic App. Sc.2012; 6: 216-226.

[12] Moon M C. Perivascular Delivery of losartan with Surgical Ffibrin Glue Prevents Neointimal Hyperplasia after Arterial Injury. Journal of vascular surgery.2004; 40.1: 130-137.

[13] Gisela T. Losartan Versus Atenolol for Prevention of Aortic Dilation in Patients with Marfan Syndrome. Journal of the American College of Cardiology.2018; 72.14: 1613-1618.

[14] Wang S F , Shen L , Tong C , Phang I Y , Lim P Q , Liu T X.Chitosan/montmorillonite nanocomposites: preparation and characterization. Polymer Degradation and Stability. Biopolymer.2005; 90(1):123-131.

[15] Casettari L, Illum L. Chitosan in nasal delivery systems for therapeutic drugs. Journal of Controlled Release. 2014;190: 189-200.

[16] Akiladvi D, Basak S.Kiladevi D. Ethosomesa Noninvasive Approach for Transdermal Drug delivery. Int J Curr Pharm Res. 2010; 2.4: 1-4.

[17] Maxwell A, Priya S .Nanosized Ethosomes–A Promising Vesicular Drug Carrier for Transdermal Drug Delivery. Research Journal of Pharmacy and Technology.2019; 12.2: 876-880.

[18] Shaikh H K, Kshirsagar R, Patil S. Mathematical models for drug release characterization: a review. WJPPS. 2015; 4, 324-338.

[19] Sun X , Sun P , Li B , Liu Y , Wang M , Suo N , Jin X. A new drug delivery system for Mitomycin C to improve intravesical instillation. Materials & Design.2016; 110: 849-857.

[20] Sun M , Su X , Ding B , He X , Liu X , Yu A , Zhai G. Advances in nanotechnology-based delivery systems for curcumin. Nanomedicine. 2012; 7(7): 1085-1100.

[21] Anitha A , Sowmya S , Kumar P S , Deepthi S , Chennazhi K , Ehrlich H , Jayakumar R. Chitin and Chitosan in Selected Biomedical Applications. Progress in Polymer Science. 2014;39(9):1644-1667.

[22] Li X , Chen S , Zhang B , Li M , Diao K , Zhang Z , Chen H. In Situ Injectable Nano-Composite Hydrogel Composed of Curcumin, N, O-carboxymethyl Chitosan and Oxidized Alginate for Wound Healing Application. International journal of pharmaceutics. 2012; 437(1):110-119.

[23] QIN Z. Transdermal Permeability of Triamcinolone Acetonide Lipid Nanoparticles. International Journal of Nanomedicine. 2019; 14: 2485-2490.

[24] Mendes I T. Development and Characterization of Nanostructured Lipid Carrier-Based Gels for the Transdermal Delivery of Donepezil. Colloids and Surfaces B: Biointerfaces. 2019; 177: 274-281.

[25] Xiaoying W , Yumin D , Jiwen L. Biopolymer/Montmorillonite Nanocomposite: Preparation, Drug-Controlled Release Property and Cytotoxicity , Nanotechnology.2008; 19 :1-7.

[26] B. Karen, J. Eun ,R. Chung, N Shah, Investigation of Soy Protein Hydrogels for Biomedical Applications: Materials Characterization, Drug Release, and Biocompatibility . Journal of Biomaterials Applications.2014; 28,1 -12.

[27] Bahri-Najafi R. Designing of the Iibuprofen Mucoadhesive Film for Relief the Oral Pain and Inflammation,. Journal of Shahrekord University of Medical Sciences. 2014; 15(6): 132-140.

[28] Silva S S , Popa E G , Gomes M E , Cerqueira M , Marques A P , Caridade S G , Reis R L . An Investigation of The Potential Application of Chitosan/Aloe-based Membranes for Regenerative Medicine. Acta Biomaterialia. 2013; 9(6), 6790-6797.

[29] Liu Y , Cai Y , Jiang X , Wu J, Le X.. Molecular Interactions, Characterization and Antimicrobial Activity of Curcumin–Chitosan Blend Films. Food Hydrocolloids. 2016; 52: 564-572.

[30] H. Hosseini, B. Shirkavand Hadavand , Synthesis and Viscoelastic Properties of Smart Hydrogel. Polymer Science, Series B. 2020 ; 62, 394 -399.

[31] YU, Meiling, et al. Intratumoral Injection of Gels Containing Iosartan Microspheres and (PLG-g-mPEG)-Cisplatin Nanoparticles Improves Drug Penetration, Retention and Anti-Tumor Activity. Cancer letters. 2019, 442: 396-408.

[32] Maxwell A ,Priya S. Nanosized Ethosomes–A Promising Vesicular Drug Carrier for Transdermal Drug Delivery. Research Journal of Pharmacy and Technology. 2019; 12.2: 876-880.

[33] Anchis R, Novel Hydrogel-Advanced Modified Clay Nanocomposites as Possible Vehicles for Drug Delivery and Controlled Release. Nanomaterials.2017; 7.12: 443-448.

[34] Wang S F, Shen L, Tong C L , Phang I Y , Lim P Q , Liu T X. Biopolymer Chitosan/Montmorillonite Nanocomposites: Preparation and Characterization. Polymer Degradation and Stability. 2005; 90(1): 123-131.

[35] Asgarzade M, Shahsavari SH . The Design of a Slow-Release Drug System, 5-Fluorouracil, Using Chitosan Magnetic Nanoparticles in the Monolute Glycerol Matrix. Iranian Journal of Pharmaceutical Research. 2018;1320-1344.

[36] Ounissa S.Optimization of Valsartan Encapsulation in Biodegradables Polyesters Using Box-Behnken Design, Materials Science and Engineering C.2018;1-10.

[37] Jha A K , Tharp K M , Ye J , Santiago-Ortiz J L , Jackson W M , Stahl A , Healy K E .Enhanced Survival and Engraftment of Transplanted Stem Cells Using Growth Factor Sequestering Hydrogels. Biomaterials. 2015; 47, 1-12.

[38] Tsai Y M , Chien C –F, Lin L C, Tsai T H. Curcumin and Its Nano-Formulation: the Kinetics of Tissue Distribution and Blood–Brain Barrier Penetration. International Journal of Pharmaceutics.2011; 416(1): 331-338.

[39] Scherf, K.Martina, B.Axel, S.André , The Contamination of Valsartan and Other Sartans, Part 2: Untargeted Screening Reveals Contamination with Amides Additionally to Known Nitrosamine Impurities. Journal of Pharmaceutical and Biomedical Analysis.2019; 172, 278 -284.